Journal of Zhejiang University-SCIENCE C (Computers & Electronics)
ISSN 1869-1951 (Print); ISSN 1869-196X (Online)
www.zju.edu.cn/jzus; www.springerlink.com
E-mail: jzus@zju.edu.cn

Using concurrent lines in central catadioptric camera calibration*

Lei ZHANG, Xin DU, Ji-lin LIU

(*Department of Information Science and Electronic Engineering, Zhejiang University, Hangzhou 310027, China*)

E-mail: ajuan.zhang@gmail.com; duxin@zju.edu.cn; liujl@zju.edu.cn

Received Mar. 2, 2010; Revision accepted June 28, 2010; Crosschecked Jan. 31, 2011

Abstract: Central catadioptric cameras have been extensively adopted in robotics and surveillance due to their extensive field of view. To attain precise 3D information in these applications, it is important to calibrate the catadioptric cameras accurately. The existing calibration techniques either require prior knowledge of the mirror types, or highly depend on a conic estimation procedure, which might be ruined if there are only small portions of the conic visible on calibration images. In this paper, we design a novel planar pattern with concurrent lines as a calibration rig, which is more robust in conic estimation since the relationship among lines is taken into account. Based on the line properties, we propose a rough-to-fine approach suitable for the new planar pattern to calibrate central catadioptric cameras. This method divides the nonlinear optimization calibration problem into several linear sub-problems that are much more robust against noise. Our calibration method can estimate intrinsic parameters and the mirror parameter simultaneously and accurately, without a priori knowledge of the mirror type. The performance is demonstrated by both simulation and a real hyperbolic catadioptric imaging system.

Key words: Catadioptric, Calibration, Concurrent lines, Conic estimation
doi:10.1631/jzus.C1000043 **Document code:** A **CLC number:** TP317.4; TP391

1 Introduction

The catadioptric camera has been recently adopted in a wide range of applications, such as robotics (Hadj-Abdelkader *et al*., 2008), 3D reconstruction (Hu, 2009; Rossi *et al*., 2009), stereo vision (Caron *et al*., 2009), and projecting devices (Ding *et al.*, 2009). As calibration is a preliminary step in most of these applications, a variety of calibration methods for catadioptric imaging systems have been reported. They differentiate themselves by the application of line properties (Geyer and Daniilidis, 2002; Ying and Hu, 2004; Barreto and Araujo, 2006), and information about the scene, such as grids (Scaramuzza *et al*., 2006; Mei and Rives, 2007; Zhang and Li, 2008; Zhang *et al*., 2009). The paracatadioptric camera is a special case in the class of catadioptric cameras. The parameter indicating the mirror type is fixed when the mirror is paraboloid. Moreover, the lines in the 3D space are projected to circles on the image, which makes the estimation of conics easier. Several algorithms have been proposed to calibrate a paracatadioptric camera. Geyer and Daniilidis (2002) presented an approach to calibrating this device from an image of merely three lines. They proposed a closed-form solution to the aspect ratio, principal point, and focal length for skewless cameras and a polynomial root solution in the presence of skew. Barreto and Araujo (2006) showed that certain properties must be verified by a set of conics to be paracatadioptric line images in uncalibrated paracatadioptric views. These properties were used to constrain the search to conics in order to obtain better conic estimation.

A more general situation is the catadioptric imaging system with a hyperboloid or ellipsoid mirror. Based on the unified projection model, properties of lines in space were well studied and inferred in Barreto and Araujo (2005). Barreto and Araujo (2002) proved that it was possible to locate both the effective viewpoint and the absolute conic in the catadioptric

* Project (Nos. 60502006, 60534070, and 90820306) supported by the National Natural Science Foundation of China

image plane from the images of three lines, and at least two lines in a hyperboloid and ellipsoid imaging system. However, the calibration algorithm for a generic central catadioptric sensor is not so desirable due to the unstable convergence in the complex nonlinear optimization. Ying and Hu (2004) introduced sphere images into calibration. They drew an important conclusion that the method based on projections of spheres is better than that of lines because of the higher accuracy of conic estimation. They used an assumption that the parameter regarding mirror type is known in both simulation and real-data experiments. Zhang *et al.* (2009) combined both the line properties and the adoption of grids. They introduced the infinity intersections of parallel lines into calibration to estimate the intrinsic parameters with a single image. They also assumed that the parameter regarding mirror type is known. Zhang and Li (2008) presented a homography-based method dealing with parabolic and hyperbolic imaging systems. They formulated the calibration task into a polynomial eigenvalue problem and obtained a closed-form solution for all variables.

In this paper, we focus on two critical problems in line-based calibration: conic estimation and mirror type parameter estimation. Generally speaking, conic is fitted by points lying on a small portion of the conic. Inspired by the conclusion in Ying and Hu (2004), we designed a novel calibration pattern with concurrent lines other than parallel lines pattern, such as chessboard. This pattern takes the relationship among the lines into consideration to enhance the constraint of concurrent lines so as to improve conic estimation accuracy. The common point of the concurrent lines is projected to be one of the intersections of the conics. Therefore, conic parameters are adjusted by varying the position of the other intersection according to line properties in an iterative procedure. Intrinsic parameters, as well as an additional parameter representing the mirror type, are estimated step by step.

2 Prerequisites

In this section we provide a brief review on a unified projection model and some projective properties of images with concurrent lines, on which our proposed calibration method is based.

2.1 Unified projection model

There are two types of model popularly used to describe all classes of the central catadioptric system. One is the Taylor series model (Scaramuzza *et al*., 2006), and the other is the unified projection model (Geyer and Daniilidis, 2000). Since the Taylor series is an approximation of hyperbola and ellipse, the Taylor series model does not describe the model precisely when the mirror section is hyperbolic or elliptic. The unified projection model fits all central catadioptric imaging systems with a hyperbolic, elliptic, or parabolic mirror. Therefore, in this study, we choose the unified projection model to represent the general case.

The unified projection model assumes that a unit sphere is centered at the origin of the world coordinate system, coincident with the focus of a reflective surface. Given an arbitrary 3D point $\boldsymbol{X}_{\mathrm{W}}=(X_{\mathrm{W}}, Y_{\mathrm{W}}, Z_{\mathrm{W}})^{\mathrm{T}}$ in the world coordinates, the mapping between $\boldsymbol{X}_{\mathrm{W}}$ and the projection point in a central catadioptric system is obtained using the following three steps:

1. The world point $\boldsymbol{X}_{\mathrm{W}}$ is first projected onto the unit sphere as $\boldsymbol{X}_{\mathrm{S}}=\boldsymbol{X}_{\mathrm{W}}/\|\boldsymbol{X}_{\mathrm{W}}\|=(X_{\mathrm{S}}, Y_{\mathrm{S}}, Z_{\mathrm{S}})^{\mathrm{T}}$.

2. The point $\boldsymbol{X}_{\mathrm{S}}$ is transferred to a new coordinate system centered at the origin $\boldsymbol{O}_{\mathrm{C}}=(0, 0, -\xi)^{\mathrm{T}}$, as depicted in Fig. 1, where $\xi=2\varepsilon/(1+\varepsilon^2)$, in which ε is the eccentricity of some given reflective surface (Table 1).

3. The point $\boldsymbol{X}_{\mathrm{S}}$ in the new coordinates is then projected to the image plane Π_{image} from $\boldsymbol{O}_{\mathrm{C}}$. It is essentially a conventional perspective projection. The perspective projection matrix $\boldsymbol{K}$ can be expressed and decomposed as

$$\boldsymbol{K}=\begin{bmatrix} f_1 & sf_2 & u_0 \\ 0 & f_2 & v_0 \\ 0 & 0 & 1 \end{bmatrix}=\boldsymbol{K}_{\mathrm{M}}\boldsymbol{K}_{\mathrm{A}}\boldsymbol{K}_{\infty}, \tag{1}$$

where s is the skew factor, (u_0, v_0) is the principal point $\hat{\boldsymbol{O}}$, (f_1, f_2) is the focal length, and $\boldsymbol{K}_{\mathrm{M}}=\begin{bmatrix} r & s & u_0 \\ 0 & 1 & v_0 \\ 0 & 0 & 1 \end{bmatrix}$, $\boldsymbol{K}_{\mathrm{A}}=\mathrm{diag}\{f_{\mathrm{e}}, f_{\mathrm{e}}, 1\}$, $\boldsymbol{K}_{\infty}=\mathrm{diag}\{1, 1, 1\}$, in which $r=f_1/f_2$, $f_{\mathrm{e}}=f_2$.

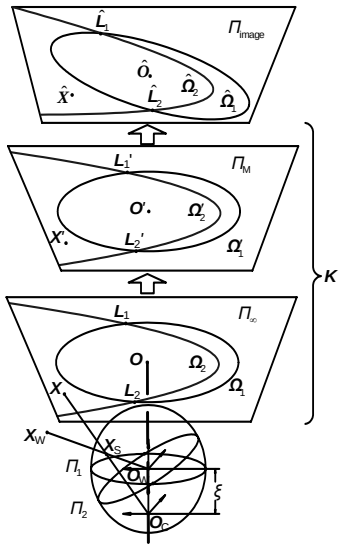

Fig. 1 The unified model for central catadioptric image formation

Π_{M} is the metric plane and Π_{image} is the image plane. A point $\boldsymbol{X}$ in the 3D space and two line images are depicted on the unit sphere, the infinite plane, the metric plane, and the image plane

Table 1 Mirror types and parameter ξ

Mirror type	ε	ξ
Planar	$\varepsilon\to\infty$	ξ=0
Elliptic	0<ε<1	0<ξ<1
Hyperbolic	ε>1	0<ξ<1
Parabolic	ε=1	ξ=1

$\xi = 2\varepsilon/(1+\varepsilon^2)$

Here we introduce the metric plane as defined in Ying and Hu (2004), with which the intrinsic parameters of a camera are as follows: r=1, s=0, u_0=0, and v_0=0. In the following, $(\cdot)^{\mathrm{T}}$ is used to denote the point coordinate, and $[\cdot]^{\mathrm{T}}$ is used to denote the line coordinate. We denote a point in the 3D space as $\boldsymbol{X}_{\mathrm{W}}$, its projection on the infinite plane Π_∞ as $\boldsymbol{X}$, its projection on the metric plane Π_{M} as $\boldsymbol{X}'$, and the projection on the image plane Π_{image} as $\hat{\boldsymbol{X}}$. For instance, in Fig. 1, the projection of a great circle on the unit sphere is denoted as

$$\boldsymbol{\Omega}=\begin{bmatrix} a & b & d \\ b & c & e \\ d & e & f \end{bmatrix} \text{ on the infinite plane } \Pi_\infty, \quad (2)$$

$$\boldsymbol{\Omega}'=\begin{bmatrix} a' & b' & d' \\ b' & c' & e' \\ d' & e' & f' \end{bmatrix} \text{ on the metric plane } \Pi_{\mathrm{M}}, \quad (3)$$

$$\hat{\boldsymbol{\Omega}}=\begin{bmatrix} \hat{a} & \hat{b} & \hat{d} \\ \hat{b} & \hat{c} & \hat{e} \\ \hat{d} & \hat{e} & \hat{f} \end{bmatrix} \text{ on the image plane } \Pi_{\mathrm{image}}. \quad (4)$$

Given a great circle on the plane Π with normal direction $\boldsymbol{n}=(n_x, n_y, n_z)^{\mathrm{T}}$, the projection on the infinite plane Π_∞ can be attained as

$$\boldsymbol{\Omega}=\begin{bmatrix} n_x^2(\xi^2-1)+n_z^2\xi^2 & n_xn_y(\xi^2-1) & -n_xn_z \\ n_xn_y(\xi^2-1) & n_y^2(\xi^2-1)+n_z^2\xi^2 & -n_yn_z \\ -n_xn_z & -n_yn_z & -n_z^2 \end{bmatrix}. \quad (5)$$

In this study, given three points $\boldsymbol{A}$, $\boldsymbol{B}$, $\boldsymbol{C}$, the length ratio of these points is denoted as $\{\boldsymbol{A},\boldsymbol{B};\boldsymbol{C}\}=(\boldsymbol{A}-\boldsymbol{C})/(\boldsymbol{B}-\boldsymbol{C})$. The cross ratio of four points $\boldsymbol{A}$, $\boldsymbol{B}$, $\boldsymbol{C}$, $\boldsymbol{D}$ is denoted as $\{\boldsymbol{A},\boldsymbol{B};\boldsymbol{C},\boldsymbol{D}\}=\{\boldsymbol{A},\boldsymbol{B};\boldsymbol{C}\}/\{\boldsymbol{A},\boldsymbol{B};\boldsymbol{D}\}$.

Generally speaking, there are two main sources of distortion in a central catadioptric imaging system (Weng and Herniou, 1992): the lens generates radial distortion, and misalignment between the camera optical center and the mirror generates both radial and tangential distortions.

A three-parameter model was chosen for the radial distortion:

$$\delta_{\rho\mathrm{d}}=1+k_1\rho^2+k_2\rho^4+k_5\rho^6, \quad (6)$$

where $\rho=\sqrt{x^2+y^2}$.

The tangential distortion can be modeled with two more parameters:

$$\boldsymbol{\delta}_{\mathrm{td}}=\begin{bmatrix} 2k_3xy+k_4(\rho^2+2x^2) \\ k_3(\rho^2+2y^2)+2k_4xy \end{bmatrix}. \quad (7)$$

The entire distortion is described by parameters k_1–k_5.

2.2 Projective properties of concurrent lines on the infinite plane

Proposition 1 A set of concurrent lines are projected onto a set of conics intersecting at two common points on the infinite plane Π_∞.

In the unified projection model, a line in the 3D space is projected to a great circle on the unit sphere. Considering three concurrent lines, their projections

on the unit sphere are three great circles which determine three planes going through the origin. If these circles intersect at a point, then their corresponding planes intersect on a line determined by the common point and the origin. This common line is also a diameter of the unit sphere. Hence, concurrent lines are projected onto a set of great circles that intersect at two antipodal points.

The normal directions of the above-mentioned great circles are coplanar on the plane Φ (Fig. 2), and the direction $\boldsymbol{BF}$ going through two common points $\boldsymbol{B}$ and $\boldsymbol{F}$ intersects the infinite plane Π_∞ at the point $\boldsymbol{L}=(l_x,\ l_y,\ l_z)^{\mathrm{T}}$. Since the common diameter is orthogonal to the normal direction of each great circle, the direction $\boldsymbol{BF}$ is orthogonal to the plane Φ.

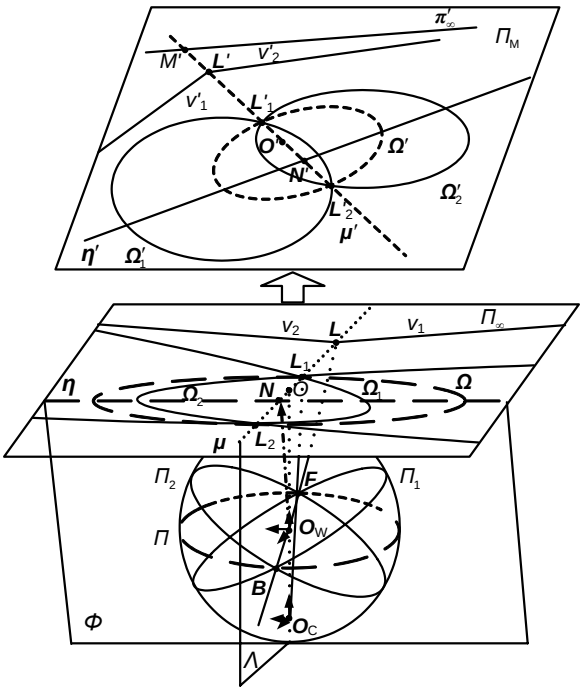

Fig. 2 The central projection image of three concurrent lines

Π_∞ denotes the plane at infinity and Π_M denotes the metric plane. Three conic curves intersect at two points $\boldsymbol{L}_1$, $\boldsymbol{L}_2$ on Π_∞, at $\boldsymbol{L}'_1$, $\boldsymbol{L}'_2$ on the metric plane Π_M. Point $\boldsymbol{O}$ is the principal point on plane Π_∞. $\boldsymbol{BF}$ is the direction of the common diameter on the unit sphere. $\boldsymbol{L}$ is the intersection of $\boldsymbol{BF}$ on the infinite plane Π_∞. $\boldsymbol{L}$, $\boldsymbol{L}_1$, $\boldsymbol{L}_2$ lie on line $\boldsymbol{\mu}$, say the projection of diameter. Line $\boldsymbol{\mu}$ and direction $\boldsymbol{BF}$ lie on plane Λ. The plane Φ of normal directions of the great circles intersects the infinite plane Π_∞ on line $\boldsymbol{\eta}$. Line $\boldsymbol{\eta}$ intersects line $\boldsymbol{\mu}$ on $\boldsymbol{N}$, which is the intersection of the normal direction of a virtual great circle Π on the infinite plane Π_∞

The polar of $\boldsymbol{L}$ with respect to the absolute conic $\boldsymbol{\Omega}_\infty$ on plane Π_∞ is the intersection line $\boldsymbol{\eta}=\boldsymbol{\Omega}_\infty\boldsymbol{L}=[l_x,\ l_y,\ l_z]^{\mathrm{T}}$ of the plane Φ (Hartley and Zisserman, 2000). $\boldsymbol{B}$ and $\boldsymbol{F}$ on the unit sphere are projected to points $\boldsymbol{L}_1=(l_x,\ l_y,\ l_z+\xi)^{\mathrm{T}}$ and $\boldsymbol{L}_2=(l_x,\ l_y,\ l_z-\xi)^{\mathrm{T}}$ on the infinite plane Π_∞ from the point $\boldsymbol{O}_C=(0,\ 0,\ -\xi)^{\mathrm{T}}$.

The line $\boldsymbol{\mu}=[l_y,\ -l_x,\ 0]^{\mathrm{T}}$ determined by the principal point $\boldsymbol{O}$ and direction point $\boldsymbol{L}$ on the infinite plane Π_∞, goes through points $\boldsymbol{L}_1$, $\boldsymbol{L}_2$, and intersects the infinite line $\boldsymbol{\pi}_\infty=[0,\ 0,\ 1]^{\mathrm{T}}$ at the point $\boldsymbol{M}=(l_x,\ l_y,\ 0)^{\mathrm{T}}$ and $\boldsymbol{\eta}$ at the point $\boldsymbol{N}=(-l_xl_z,\ -l_xl_z,\ l_x^2+l_y^2)^{\mathrm{T}}$. $\boldsymbol{N}$ is the intersection of the normal direction of a virtual great circle Π on the infinite plane Π_∞. Plane Λ defined by direction $\boldsymbol{BF}$ and line $\boldsymbol{O}_W\boldsymbol{O}$ is symmetric to the virtual great circle Π. Conic $\boldsymbol{\Omega}$ is the projection of Π on plane Π_∞. Since Λ intersects Π_∞ on line $\boldsymbol{\mu}$, evidently, conic $\boldsymbol{\Omega}$, whose direction is $\boldsymbol{N}$, is symmetric about line $\boldsymbol{\mu}$ on Π_∞. By replacing the normal direction in Eq. (5) with $\boldsymbol{N}$, the projection of the virtual great circle Π on the infinite plane Π_∞ can be obtained. By definition, the center $\boldsymbol{C}$ of $\boldsymbol{\Omega}$ is the pole of the infinite line $\boldsymbol{\pi}_\infty$ with respect to $\boldsymbol{\Omega}$. The center of $\boldsymbol{\Omega}$ could be obtained as $\boldsymbol{C}=\boldsymbol{\Omega}^*\boldsymbol{\pi}_\infty=(l_xl_z,\ l_yl_z,\ l_z^2-\xi^2)^{\mathrm{T}}$, where $\boldsymbol{\Omega}^*$ is the dual figure of $\boldsymbol{\Omega}$. We obtain the expressions of points $\boldsymbol{L}_1$, $\boldsymbol{L}_2$, and $\boldsymbol{C}$, which subsequently lead to the following proposition:

Proposition 2 The length ratio of $\boldsymbol{C}$ with respect to $\{\boldsymbol{L}_1, \boldsymbol{L}_2\}$ is invariant under affine transformation:

$$\{\boldsymbol{L}_1, \boldsymbol{L}_2; \boldsymbol{C}\} = -1. \tag{8}$$

A pair of points $\{\boldsymbol{C}, \boldsymbol{M}\}$ is harmonic conjugate with respect to $\{\boldsymbol{L}_1, \boldsymbol{L}_2\}$ (Barreto, 2003). According to the definition of 'conic diameter' in Semple and Kneebone (1952), line $\boldsymbol{\Omega}_i\boldsymbol{M}$ is a diameter of conic $\boldsymbol{\Omega}_i$. Since $\boldsymbol{L}_1$ and $\boldsymbol{L}_2$ are the common intersections of each conic $\boldsymbol{\Omega}_i$, lying on the line $\boldsymbol{\mu}$, the center $\boldsymbol{C}$ of conic $\boldsymbol{\Omega}$ is on the intersection of line $\boldsymbol{\Omega}_i\boldsymbol{M}$ and $\boldsymbol{\mu}$.

$$\boldsymbol{C} = \boldsymbol{\mu} \wedge (\boldsymbol{\Omega}_i\boldsymbol{M}). \tag{9}$$

Note that projective transformation maintains the cross ratio and relations of lines and points, as depicted in Fig. 2. Hence, all above-introduced expressions stay valid on the image plane except Eq. (8), which remains valid under affine transformation.

3 Calibration with concurrent lines

Based on the unified projection model introduced in Section 2.1, the calibration of central catadioptric cameras is used to estimate the six parameters $\{s, u_0, v_0, f_1, f_2, \xi\}$. In previous line-based calibration methods, usually the first step is to calculate the intersections of conics, which highly rely on the accuracy of the conics estimation, followed by a global optimization, such as the Levenberg-Marquardt algorithm. The global optimization requires initial values be close to true values. Otherwise, it easily gets stuck in local optima. However, in practice, either noise or only a small portion of the conic would easily ruin the relative positions of the conics.

In view of the properties specific to concurrent lines, we propose a rough-to-fine framework that first estimates conics and initializes the camera parameters, second rectifies the conics and refines all of the parameters according to line properties and the propositions proposed in this study, and finally optimizes the parameters by minimizing the reprojection error of the corners with a global optimization. By this means, an essential nonlinear optimization problem is split into several linear sub-problems so that the calibration is more tolerant to noises.

3.1 Initialization of the parameters

In most catadioptric systems, which are combined with reflective mirrors and commercial cameras, the cameras are aligned well with the reflective surfaces, and $\boldsymbol{K}$ is an affine transformation. On the metric plane Π_{M}, the mirror boundary is perpendicular to the optical axis of the camera; hence, the boundary is supposed to be a circle if the coordinates of the image plane are orthogonal to each other. As shown in Ying and Hu (2004), an ellipse is fitted to the boundary in order to initialize the principal point while the aspect ratio and the skew factor are initialized as r=1 and s=0, respectively (Mei and Rives, 2007).

$$u_0 = \frac{\hat{b}\hat{e} - \hat{c}\hat{d}}{\hat{a}\hat{c} - \hat{b}^2}, \quad v_0 = \frac{\hat{b}\hat{d} - \hat{c}\hat{e}}{\hat{a}\hat{c} - \hat{b}^2}, \tag{10}$$

where $\hat{a}\cdots\hat{e}$ are as defined in Eq. (4). Now, we obtain the initial guess of parameters $r=f_1/f_2$, s, u_0, and v_0. The focal length f_{e} and mirror type parameter ξ will be initialized by exploiting the line properties reported in Barreto (2003). A linear approach is proposed for estimating focal length f_{e} and mirror type parameter ξ.

In Fig. 2, $\boldsymbol{v}_i$ (i=1, 2) is the polar line of $\boldsymbol{O}$ with respect to $\boldsymbol{\Omega}_i$, and $\boldsymbol{\mu}$ is the line going through two intersection points $\boldsymbol{L}_1$ and $\boldsymbol{L}_2$. Then $\boldsymbol{v}_i$ and $\boldsymbol{\mu}$ intersect at the same point $\boldsymbol{L}$ (Barreto, 2003). Considering Proposition 1, on the image plane Π_{image}, the polar lines of $\hat{\boldsymbol{O}}$ with respect to each conic $\hat{\boldsymbol{\Omega}}_i$ go through the same point $\hat{\boldsymbol{L}}$. Therefore, projection of direction $\boldsymbol{L}$ on the image plane can be linearly solved by

$$\left[\hat{\boldsymbol{\Omega}}_1\hat{\boldsymbol{O}},\ \hat{\boldsymbol{\Omega}}_2\hat{\boldsymbol{O}},\ \cdots,\ \hat{\boldsymbol{\Omega}}_i\hat{\boldsymbol{O}}\right]^{\mathrm{T}}\hat{\boldsymbol{L}} = \boldsymbol{0}. \tag{11}$$

Then, we obtain $\hat{\boldsymbol{\mu}}$ which goes through two intersections $\hat{\boldsymbol{L}}_1$ and $\hat{\boldsymbol{L}}_2$ as well as $\hat{\boldsymbol{O}}$ and $\hat{\boldsymbol{L}}$. $\hat{\boldsymbol{M}}$ is the intersection of lines $\hat{\boldsymbol{\mu}}$ and $\hat{\boldsymbol{\pi}}_\infty = [0, 0, 1]^{\mathrm{T}}$. Diameter of each conic $\hat{\boldsymbol{\Omega}}_i$ is the polar of $\hat{\boldsymbol{M}}$ with respect to each conic. Considering Eq. (9), every diameter $\hat{\boldsymbol{\Omega}}_i\hat{\boldsymbol{M}}$ goes through the center $\hat{\boldsymbol{C}}$ of conic $\hat{\boldsymbol{\Omega}}$. Hence, we obtain

$$\left[\hat{\boldsymbol{\Omega}}_1\hat{\boldsymbol{M}},\ \hat{\boldsymbol{\Omega}}_2\hat{\boldsymbol{M}},\ \cdots,\ \hat{\boldsymbol{\Omega}}_i\hat{\boldsymbol{M}}\right]^{\mathrm{T}}\hat{\boldsymbol{C}} = \boldsymbol{0}. \tag{12}$$

If conic $\boldsymbol{\Omega}_i$ is a line image going through points $\boldsymbol{L}_1$, $\boldsymbol{L}_2$, then the pole of $\boldsymbol{\mu}$ with respect to $\boldsymbol{\Omega}_i$ lies on $\boldsymbol{\eta}$ (Barreto, 2003). Since the pole of $\hat{\boldsymbol{\mu}}$ with respect to each conic $\hat{\boldsymbol{\Omega}}_i$ lies on $\hat{\boldsymbol{\eta}}$, the projection of horizon line $\hat{\boldsymbol{\eta}}$ is also a linear solution of homogeneous equations:

$$\left[\hat{\boldsymbol{\Omega}}_1^*\hat{\boldsymbol{\mu}},\ \hat{\boldsymbol{\Omega}}_2^*\hat{\boldsymbol{\mu}},\ \cdots,\ \hat{\boldsymbol{\Omega}}_i^*\hat{\boldsymbol{\mu}}\right]^{\mathrm{T}}\hat{\boldsymbol{\eta}} = \boldsymbol{0}, \tag{13}$$

where $\hat{\boldsymbol{\Omega}}_i^*$ is the dual figure of $\hat{\boldsymbol{\Omega}}_i$. As shown in Fig. 2, we obtain point $\hat{\boldsymbol{N}}$ by intersecting lines $\hat{\boldsymbol{\mu}}$ and $\hat{\boldsymbol{\eta}}$.

$\hat{\boldsymbol{L}}$ and $\hat{\boldsymbol{N}}$ have been obtained on the image plane. Their correspondences on the metric plane in the Cartesian coordinates are

$$\boldsymbol{L}' = \boldsymbol{K}_{\mathrm{M}}^{-1}\hat{\boldsymbol{L}} = \left(\frac{l_x f_{\mathrm{e}}}{l_z},\ \frac{l_y f_{\mathrm{e}}}{l_z}\right)^{\mathrm{T}}, \tag{14}$$

$$\boldsymbol{N}' = \boldsymbol{K}_{\mathrm{M}}^{-1}\hat{\boldsymbol{N}} = \left(-\frac{l_x l_z}{l_x^2 + l_y^2} f_{\mathrm{e}},\ -\frac{l_y l_z}{l_x^2 + l_y^2} f_{\mathrm{e}}\right)^{\mathrm{T}}. \tag{15}$$

Hence, the focal length can be derived from Eqs. (14) and (15) on the metric plane and we choose the mean value:

$$f_{\mathrm{e}}=\mathrm{mean}\left(\sqrt{\frac{-\left\|\boldsymbol{K}_{\mathrm{M}}^{-1}\hat{\boldsymbol{L}}\right\|^{2}\boldsymbol{K}_{\mathrm{M}}^{-1}\hat{\boldsymbol{N}}}{\boldsymbol{K}_{\mathrm{M}}^{-1}\hat{\boldsymbol{L}}}}\right),\tag{16}$$

where the operator mean() takes the mean value of the elements of the vector. For example, for an n-element vector $\boldsymbol{a}$, mean($\boldsymbol{a}$)=(a_1+a_2+…+a_n)/n. The division in Eq. (16) indicates the division among the corresponding elements.

Barreto (2003) proved that the cross ratio among points $\boldsymbol{O}$, $\boldsymbol{L}$, $\boldsymbol{N}$, and $\boldsymbol{C}$ is invariant, depending only on the shape of the reflective surface, so that {$\boldsymbol{O}$, $\boldsymbol{L}$; $\boldsymbol{N}$, $\boldsymbol{C}$}=ξ^2. This expression is invariant under projective transformation. Hence, ξ can be estimated by

$$\xi=\sqrt{\left\{\hat{\boldsymbol{O}},\hat{\boldsymbol{L}};\hat{\boldsymbol{N}},\hat{\boldsymbol{C}}\right\}}.\tag{17}$$

3.2 Step-by-step calibration

On the image plane Π_{image}, $\hat{\boldsymbol{L}}_1$ (which is the common point of concurrent lines) is a prerequisite in our proposed algorithm. The other common point is required to rectify inaccurately estimated concurrent conics. Considering Proposition 2, since $\boldsymbol{K}$ is an affine transformation, the length ratio is invariant on the image plane Π_{image}. $\hat{\boldsymbol{L}}_2$ can be calculated using Eq. (8) when $\hat{\boldsymbol{L}}_1$ and $\hat{\boldsymbol{C}}$ are known.

All of the conics $\hat{\boldsymbol{\Omega}}_i$ are supposed to go through these two common points; hence, $\hat{\boldsymbol{\Omega}}_i$ can be re-estimated by adding the second intersection. Subsequently, points $\hat{\boldsymbol{L}}$, $\hat{\boldsymbol{C}}$ and line $\hat{\boldsymbol{\eta}}$ are updated by Eqs. (11), (12), and (13), respectively. However, the estimated second intersection may not be in a correct position. As shown in Fig. 3, the estimated conics fit the extracted corners very well, but do not fit the lines on the calibration pattern precisely. Therefore, we introduce a constraint on the metric plane.

Proposition 3 On the metric plane Π_{M}, line $\boldsymbol{\mu}'$ is perpendicular to line $\boldsymbol{\eta}'$.

$$(\boldsymbol{K}_{\mathrm{M}}^{\mathrm{T}}\hat{\boldsymbol{\mu}})^{\mathrm{T}}\boldsymbol{\Omega}_{\infty}\boldsymbol{K}_{\mathrm{M}}^{\mathrm{T}}\hat{\eta}=0,\tag{18}$$

where $\boldsymbol{\Omega}_{\infty}$=diag{1, 1, 0}.

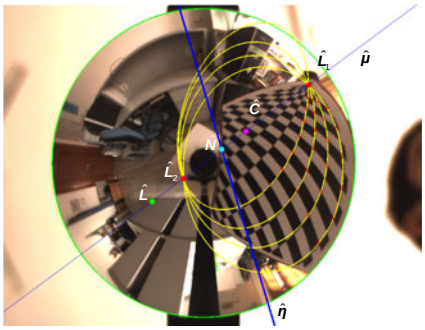

Fig. 3 Re-estimation of conics with two common intersections

Since $\boldsymbol{BF}$ is orthogonal to the plane Φ and the symmetric axis $\boldsymbol{OO}_{\mathrm{C}}$ is also orthogonal to the plane Π_{∞}, the horizon line $\boldsymbol{\eta}$ of plane Φ is orthogonal to the plane Λ where the line $\boldsymbol{\mu}$ lies. $\boldsymbol{K}_{\mathrm{A}}$ is a similarity transform; hence, the relation remains on the metric plane. To minimize the cost function

$$E=(\boldsymbol{K}_{\mathrm{M}}^{\mathrm{T}}\hat{\boldsymbol{\mu}})^{\mathrm{T}}\Omega_{\infty}\boldsymbol{K}_{\mathrm{M}}^{\mathrm{T}}\hat{\boldsymbol{\eta}}\tag{19}$$

according to the criterion of Eq. (18), we vary the common point $\hat{\boldsymbol{L}}_2$ along the line $\hat{\boldsymbol{\mu}}$ on the image plane Π_{image}, to re-estimate the parameters of a set of conics $\hat{\boldsymbol{\Omega}}_i$. Direction $\hat{\boldsymbol{L}}$, $\hat{\boldsymbol{N}}$ and center $\hat{\boldsymbol{C}}$ of conic $\hat{\boldsymbol{\Omega}}$ are re-estimated. Then, the mirror parameter ξ and focal length f_{e} are updated by Eqs. (17) and (16) respectively, until the cost function $E=(\boldsymbol{K}_{\mathrm{M}}^{\mathrm{T}}\hat{\boldsymbol{\mu}})^{\mathrm{T}}\Omega_{\infty}\boldsymbol{K}_{\mathrm{M}}^{\mathrm{T}}\hat{\boldsymbol{\eta}}$ is less than a given threshold ε. Fig. 4 shows the result of the rectification. The conics better fit the lines on concurrent lines pattern compared with Fig. 3 when line $\hat{\boldsymbol{\mu}}$ is adjusted to be orthogonal to line $\hat{\boldsymbol{\eta}}$ on the metric plane Π_{M}.

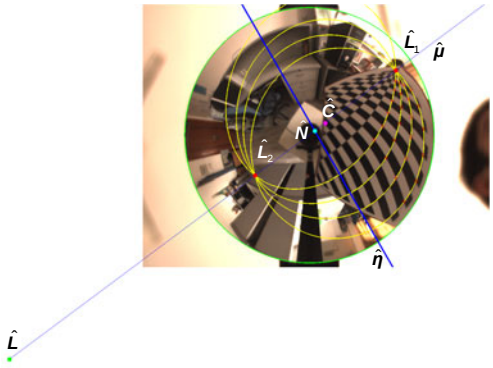

Fig. 4 Rectifying the conic according to Proposition 3 by varying the position of $\hat{\boldsymbol{L}}_2$

3.3 Global optimization

The intrinsic parameters s, u_0, v_0, f_1, f_2 and mirror type parameter ξ are obtained. The coordinate of the corner $\boldsymbol{X}_{\mathrm{P}}$ on the calibration pattern is a preliminary knowledge. Thus, we can project the corners on the calibration pattern onto the image plane.

$$\boldsymbol{X}_{\mathrm{W}} = \boldsymbol{R}\boldsymbol{X}_{\mathrm{P}} + \boldsymbol{T}, \quad \lambda\tilde{\boldsymbol{m}} = \boldsymbol{K}\left(\frac{\boldsymbol{X}_{\mathrm{W}}}{\|\boldsymbol{X}_{\mathrm{W}}\|} - \boldsymbol{O}_{\mathrm{C}}\right),$$

where λ is a scale factor. The error between the reprojecting point and the corners extracted on the image can be minimized by a global optimization. Therefore, by reprojecting the point of concurrent lines onto the image plane, we perform a global optimization such as the Levenberg-Marquardt algorithm to improve the intrinsic parameters s, u_0, v_0, f_1, f_2 and the mirror type parameter ξ. The main procedure of the proposed approach is summarized as Algorithm 1.

Algorithm 1 Main procedure of the proposed approach

Initialization

1. Estimate all of the conics on an image.
2. Initialize r=1, s=0, and the principal point (u_0, v_0) with the mirror boundary (Eq. (10)).
3. Compute the direction point $\hat{\boldsymbol{L}}$ (Eq. (11)), line $\hat{\boldsymbol{\mu}}$, point $\hat{\boldsymbol{M}}$, the center $\hat{\boldsymbol{C}}$ of conic $\hat{\boldsymbol{\Omega}}$ (Eq. (12)), line $\hat{\boldsymbol{\eta}}$ (Eq. (13)), and point $\hat{\boldsymbol{N}}$.
4. Initialize focal length f_{e} (Eq. (16)) and mirror parameter ξ (Eq. (17)).

Step-by-step calibration

5. Compute $\hat{\boldsymbol{L}}_2$ (Eq. (8)) and update point $\hat{\boldsymbol{L}}$ (Eq. (11)), $\hat{\boldsymbol{C}}$ (Eq. (12)) and line $\hat{\boldsymbol{\eta}}$ (Eq. (13)).
6. Re-estimate all conics $\hat{\boldsymbol{\Omega}}_i$.
7. Update direction $\hat{\boldsymbol{L}}$ (Eq. (11)), center $\hat{\boldsymbol{C}}$ (Eq. (12)), lines $\hat{\boldsymbol{\mu}}$, $\hat{\boldsymbol{\eta}}$ (Eq. (13)), and point $\hat{\boldsymbol{N}}$.
8. Update focal length f_{e} (Eq. (16)) and mirror parameter ξ (Eq. (17)).
9. If the cost function $E = (\boldsymbol{K}_{\mathrm{M}}^{\mathrm{T}}\hat{\boldsymbol{\mu}})^{\mathrm{T}}\boldsymbol{\Omega}_{\infty}\boldsymbol{K}_{\mathrm{M}}^{\mathrm{T}}\hat{\boldsymbol{\eta}}$ is not less than a given threshold ε, vary the common point $\hat{\boldsymbol{L}}_2$ along the line $\hat{\boldsymbol{\mu}}$, and go to line 6.

Global optimization

10. Minimize the reprojection error of the corners to optimize the parameters s, u_0, v_0, f_1, f_2, and ξ.

4 Experiments

The calibration of a central catadioptric imaging system is usually formulized as a nonlinear optimization problem whose performance relies on the accuracy of input data and the convexity of the designed cost function. In reality, calibration algorithms always suffer from noise, for instance, system noise and quantization errors, so does the estimation of conics used in most of line-based calibration algorithms. In Ying and Hu (2004), line images were obtained either by detecting edges in real-data experiments or by choosing 100 points on each projection curve in simulation. For convenience, we designed a special calibration rig (Fig. 5). Corners were detected and hence points on concurrent lines were attained. Ten points were simulated for each line to imitate the planar pattern. An assumption adopted by most current off-shelf cameras is that the two axes on the image plane are orthogonal; that is to say, the skew factor s is assumed to be 0.

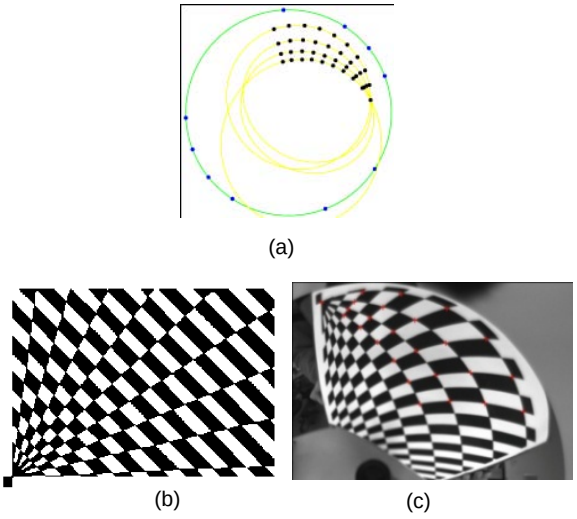

(a) (b) (c)

Fig. 5 Calibration pattern

(a) Concurrent line pattern, with curves indicating the estimated conics; (b) Simulated pattern; (c) Concurrent line pattern captured by a central catadioptric imaging system

Barreto and Araujo (2002) provided a toolbox for the parabolic central catadioptric camera. Their method worked very well with the images captured by the parabolic central catadioptric sensor. A toolbox for a generic central catadioptric camera was also provided. However, the algorithm cannot easily converge due to the expensive and complex nonlinear

optimization. Mei and Rives (2007) provided a toolbox that can work with all types of central catadioptric system, such as parabolic and hyperbolic/ellipse sensors. We compare our method with the method proposed by Mei and Rives (2007).

4.1 Synthetic data

In the simulation, the central catadioptric system was designed to have the following parameters: r=1, s=0, u_0=500, v_0=500, f_e=300, and ξ=0.9, and the image resolution ws 1000×1000. Conic estimation is of great importance in calibration. To simplify the experiment, we assumed the line images are ellipse (or circle), since in practice most of the conics are ellipse (or circle). Here, we used an ellipse-specific method called least squares fitting of ellipses (Fitzgibbon and Pilu, 1999).

The projection of the mirror boundary was generated on the image in simulation, while it was manually selected in real data experiments. The boundary was represented by 10 separated points randomly located along the entire boundary. Four concurrent lines composed the simulated pattern. On each image, the simulated pattern rotated inside of the boundary. A small and random vector was added to the position of the simulated pattern. On each projection curve, we chose 10 points on a quarter of the entire conic (Fig. 3a) with Gaussian noise of 0 mean and σ standard deviation. Deviation σ was varied from 0.5 to 2.0 pixels with a step of 0.5 pixels, and the number of images was varied from 2 to 6 with a step of 2. For each case, the mean value and standard deviation of the parameters were calculated and 1000 independent trials were conducted. The results are shown in Fig. 6a−6e. In Fig. 6f, we varied the number of images from 1 to 10. For each number, 1000 independent trials of noise with mean 0 and standard deviation 1 pixel were conducted.

Fig. 6 shows the results of synthetic data including the estimation of u_0, v_0, f_1, f_2, r, and ξ. The standard deviations of estimation results were proportional to the noise levels, while the mean value deviated to the ground truth decreased with the increase of the number of images. The mean values of u_0 (Fig. 6a) and v_0 (Fig. 6b) were less influenced than other three parameters by the noises. The main reason for this may be due to the centrosymmetry of the catadioptric image. f_1 and f_2 are related by ratio r; hence, the results in Figs. 6c and 6d were similar. Fig. 6f shows that the mean error and standard deviation of the estimated parameters decreased when more images were used. The proposed method achieved a result with a single image; however, the relative error was much larger than when the number of images was more than one (Fig. 6f). The relative errors decreased slowly when the image number was more than 5.

4.2 Real experiments

The central catadioptric camera we used consists of a hyperbolic mirror of ε=1.3017 (http://www.neovision.cz/prods/panoramic/h3s.html) with a Sony XCD-SX910CR camera (Sony, Japan). We took ξ=0.9662 as a ground truth. The concurrent lines were extracted from the planar pattern. The resolution of these images was 1280×960 pixels. Since six points are the minimal requirement in conic estimation (Fitzgibbon and Pilu, 1999), we extracted seven points on conics and six points on mirror boundaries by clicking on the corner of the planar pattern and the edge of the mirror, respectively. For each image, four or five lines were selected, when three lines are the minimal requirement for solving a homogeneous equation such as Eqs. (11)−(13). All of the corners had sub-pixel precision.

Mei and Rives (2007) considered only the first two coefficients of radial distortion and ignored the tangential distortion in the experiment of hyperbolic sensor calibration. Since the imaging system is centrosymmetric to the optical axis, the variation of the mirror parameter ξ affects the projection point along the radial direction. As described in Section 2.1, the image point can be expressed as $\lambda\boldsymbol{m}=\boldsymbol{K}(\boldsymbol{X}_S-\boldsymbol{O}_C)$. The image point $\boldsymbol{m}(u, v)$ can be obtained by

$$u=\frac{f_1X_S+sf_2Y_S}{Z_S+\xi}+u_0,\quad v=\frac{f_2Y_S}{Z_S+\xi}+v_0.$$

Considering the radial distortion in Eq. (6), the parameter ρ is related to mirror type parameter ξ:

$$\begin{aligned}\rho^2&=(u-u_0)^2+(v-v_0)^2\\&=\begin{bmatrix}f_1 & sf_2\\ 0 & f_2\end{bmatrix}\begin{bmatrix}X_S\\ Y_S\end{bmatrix}\frac{1}{(Z_S+\xi)^2}.\end{aligned}$$

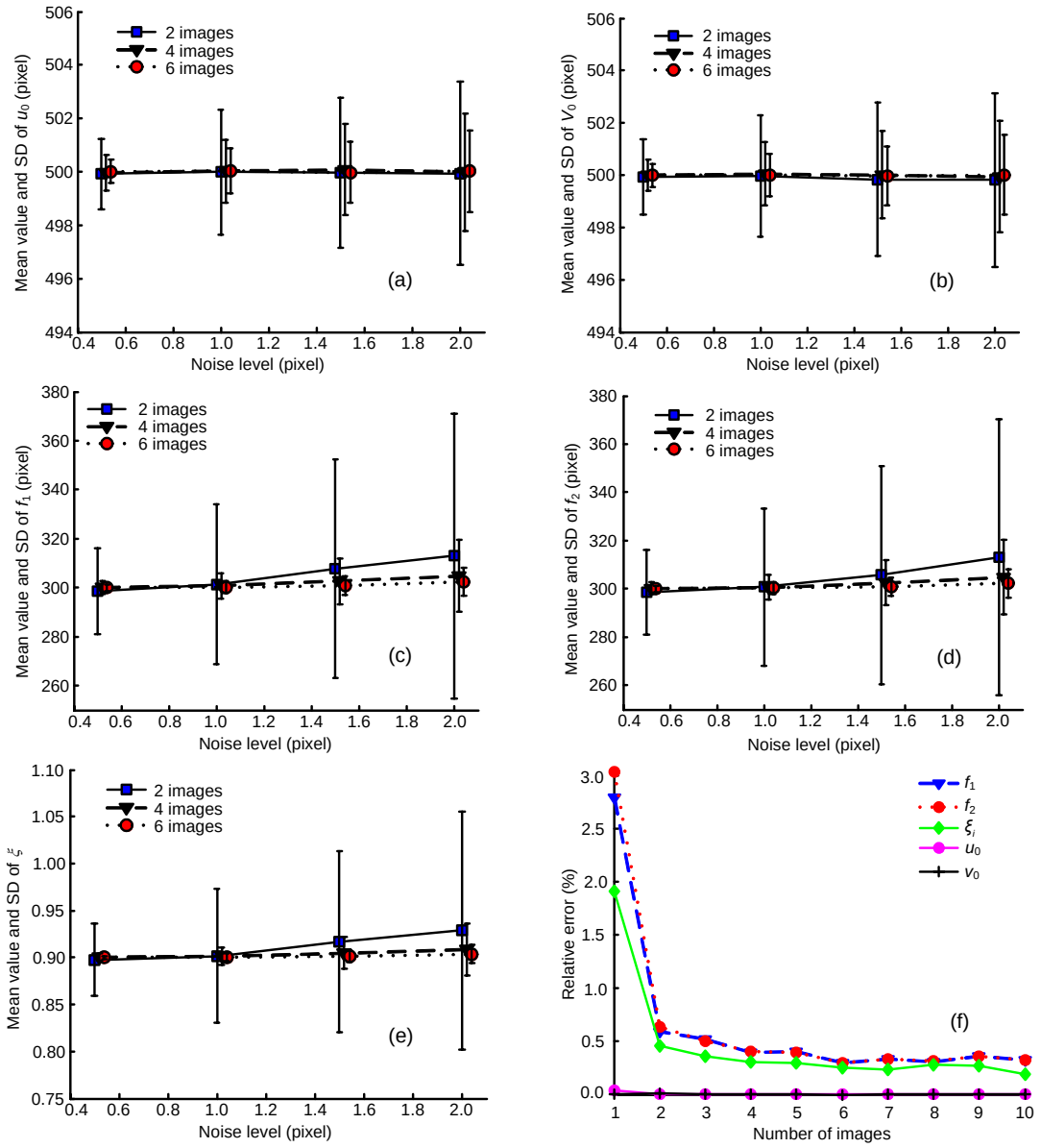

Fig. 6 Simulation results

Mean value and standard deviation (SD) of estimated parameters including u_0, v_0, f_1, f_2, r, and ξ are plotted in (a), (b), (c), (d), and (e), respectively; (f) is the relative error of the parameters with a noise of mean 0 and standard deviation 1 pixel, when the number of images varies. For each number of images, 1000 independent trials of noise with mean 0 and standard deviation 1 pixel were conducted. The vertical lines are standard deviations

Therefore, the radial distortion can be considered as a function of the mirror parameter ξ, but the tangential distortion cannot. For robustness, in the experiment with real data, only the coefficients of tangential distortion were estimated. The calibration results of the proposed method with six images are listed in Table 2. We compared our method with the toolbox provided in Mei and Rives (2007) with different input data. The results of Mei's toolbox with chessboard pattern are listed in Table 3, where about 50 corners were extracted from the chessboard image according to the toolbox's instruction, and concurrent line patterns are listed in Table 4, where the input data was the same as in Table 3. These results show that the difference among the three cases was the estimation of focal lengths f_1, f_2 and mirror parameter ξ.

When the value of ξ was overestimated (Table 3), the value of focal length was proportional to ξ, and vice versa (Table 4). Tables 3 and 4 show that concurrent lines pattern improved the estimation of both focal lengths and ξ. The refining steps regarding the propositions reported in this study make the mirror parameter closer to the ground truth, according to Tables 2 and 4.

Table 2 Results of the proposed method with concurrent lines pattern*

Parameter	Result	3σ
(u_0, v_0)	(638.25, 472.08)	(0.2267, 0.2523)
(f_1, f_2)	(333.93, 334.09)	(1.2295, 1.1304)
ξ	0.9618	0.0031
(k_3, k_4)	(0.0085, −0.0076)	
(e_u, e_v)	(0.6386, 0.6473)	

* Ground truth: 0.9662. (e_u, e_v) indicates the reprojection error in pixel and 3σ indicates the uncertainty of the results

Table 3 Results of Mei and Rives (2007)'s toolbox with chessboard pattern*

Parameter	Result	3σ
(u_0, v_0)	(639.37, 472.85)	(1.6451, 1.3889)
(f_1, f_2)	(372.13, 372.62)	(26.6492, 26.6576)
ξ	1.1860	0.1555
(k_3, k_4)	(0.0133, −0.0129)	
(e_u, e_v)	(0.2138, 0.1835)	

* Ground truth is 0.9662, and about 50 corners were extracted from the chessboard image. (e_u, e_v) indicates the reprojection error in pixel and 3σ indicates the uncertainty of the results

Table 4 Results of Mei and Rives (2007)'s toolbox with concurrent lines pattern*

Parameter	Result	3σ
(u_0, v_0)	(639.16, 474.92)	(0.2556, 0.3214)
(f_1, f_2)	(323.45, 325.25)	(2.0346, 2.1168)
ξ	0.9481	0.0053
(k_3, k_4)	(0.0115, −0.0020)	
(e_u, e_v)	(0.7871, 0.6813)	

* Ground truth: 0.9662. (e_u, e_v) indicates the reprojection error in pixel and 3σ indicates the uncertainty of the results

There are several ways of unwrapping a panoramic image by projecting from a sphere to a different surface, such as cylinder, six-face cube, and four-face cube. In this study, we exploited cubic projection for mapping a portion of the surface of a sphere to flat images, which causes a minimal distance from the sphere surface. Assuming that the catadioptric camera provides vertically a 212° FOV (a vertical field of view from the left side of the mirror to the right side), the panoramic image is unwrapped onto five flat surfaces. Four cube faces cover front, right, back, and left, as well as one more for the nadir, each having 90°×90° FOV (Fig. 7). In the left view of the unwrapped image, lines on the pattern which is conic in the panoramic image are rectified to straight lines; for example, the left first line fits the straight line in Fig. 7d. We can see that the line on the unwrapped image is not straight (Fig. 7e), if the calibration result is inaccurate.

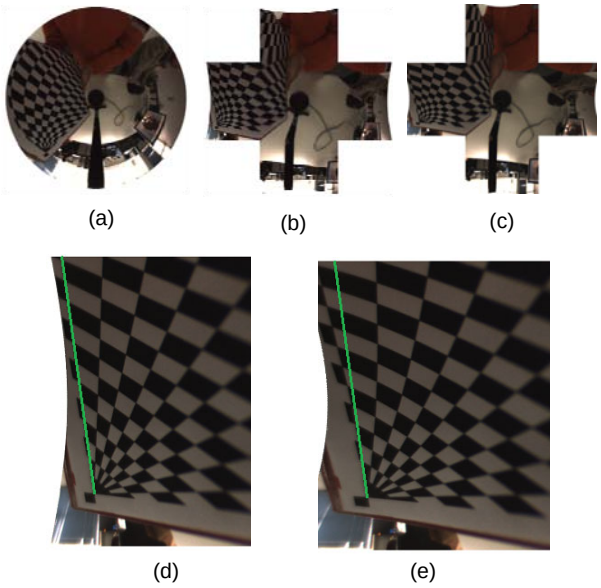

Fig. 7 Rectification of a central catadioptric image
(a) The original panoramic image acquired by a catadioptric camera; (b) Unwrapped image in five views of a cube by cubic projection using the results in Table 2; (c) Unwrapped image in five views of a cube by cubic projection using the results in Table 3; (d) Left view of (b); (e) Left view of (c). The straight line is used to check out the straightness of the rectified lines on concurrent lines pattern

5 Conclusions

In this paper we propose a rough-to-fine approach to calibrating central catadioptric cameras based on projection properties of line images. This method divides the nonlinear optimization calibration problem into several linear sub-problems that are much more robust against noise. We also design a planar pattern with concurrent lines as a calibration rig, which makes it convenient to obtain image points

on concurrent lines. Conic estimation, as the most important part of line-based calibration methods, is more robust using concurrent lines since the relationship among lines is taken into account. Without a priori knowledge of the mirror type, our calibration method can be used to estimate intrinsic parameters and the mirror parameter simultaneously and accurately. The effectiveness of the algorithm is validated by both simulation and a real hyperbolic catadioptric imaging system.

References

Barreto, J., 2003. General Central Projection System Modelling, Calibration and Visual Servoing. PhD Thesis, University of Coimbra, Coimbra, Portugal.

Barreto, J., Araujo, H., 2002. Geometric Properties of Central Catadioptric Line Images and Their Application in Calibration. European Conf. on Computer Vision, p.237-251. [doi:10.1007/s11263-007-0082-8]

Barreto, J., Araujo, H., 2005. Geometric properties of central catadioptric line images and their application in calibration. *IEEE Trans. Pattern Anal. Mach. Intell.*, **27**(8):1327-1333. [doi:10.1109/TPAMI.2005.163]

Barreto, J., Araujo, H., 2006. Fitting conics to paracatadioptric projections of lines. *Comput Vis. Image Understand.*, **101**(3):151-165. [doi:10.1016/j.cviu.2005.07.002]

Caron, G., Marchand, E., Mouaddib, E.M., 2009. 3D Model Based Pose Estimation for Omnidirectional Stereovision. IEEE/RSJ Int. Conf. on Intelligent Robots and Systems, p.5228-5233. [doi:10.1109/IROS.2009.5353955]

Ding, Y., Xiao, J., Tan, K., Yu, J., 2009. Catadioptric Projectors. IEEE Conf. on Computer Vision and Pattern Recognition, p.2528-2535. [doi:10.1109/CVPR.2009.5206622]

Fitzgibbon, R., Pilu, M., 1999. Direct least square fitting of ellipses. *IEEE Trans. Pattern Anal. Mach. Intell.*, **21**(5):476-480. [doi:10.1109/34.765658]

Geyer, C., Daniilidis, K., 2000. A Unifying Theory for Central Panoramic Systems and Practical Implications. European Conf. on Computer Vision, p.455-461.

Geyer, C., Daniilidis, K., 2002. Paracatadioptric camera calibration. *IEEE Trans. Pattern Anal. Mach. Intell.*, **24**(5):687-695. [doi:10.1109/34.1000241]

Hadj-Abdelkader, H., Mezouar, Y., Martinet, P., Chaumette, F., 2008. Catadioptric visual servoing from 3-D straight lines. *IEEE Trans. Robot.*, **24**(3):652-665. [doi:10.1109/TRO.2008.919288]

Hartley, R., Zisserman, A., 2000. Multiple View Geometry in Computer Vision. Cambridge University Press, New York, NY, USA. [doi:10.2277/0521540518]

Hu, B., 2009. It's All Done with Mirrors: Calibration-and-Correspondence-Free 3D Reconstruction. Canadian Conf. on Computer and Robot Vision, p.148-154. [doi:10.1109/CRV.2009.29]

Mei, C., Rives, P., 2007. Single View Point Omnidirectional Camera Calibration from Planar Grids. IEEE Int. Conf. on Robotics and Automation, p.3945-3950. [doi:10.1109/ROBOT.2007.364084]

Rossi, R., Savatier, X., Ertaud, J.Y., Mazari, B., 2009. Real-Time 3D Reconstruction for Mobile Robot Using Catadioptric Cameras. IEEE Int. Workshop on Robotic and Sensors Environments, p.104-109. [doi:10.1109/ROSE.2009.5355981]

Scaramuzza, R., Martinelli, A., Siegwart, R., 2006. A Flexible Technique for Accurate Omnidirectional Camera Calibration and Structure from Motion. IEEE Int. Conf. on Computer Vision Systems, p.45-52. [doi:10.1109/ICVS.2006.3]

Semple, J., Kneebone, G., 1952. Algebraic Projective Geometry. Oxford University Press, Oxford.

Weng, P., Herniou, M., 1992. Camera calibration with distortion models and accuracy evaluation. *IEEE Trans. Pattern Anal. Mach. Intell.*, **14**(10):965-980. [doi:10.1109/34.159901]

Ying, X., Hu, Z., 2004. Catadioptric camera calibration using geometric invariants. *IEEE Trans. Pattern Anal. Mach. Intell.*, **26**(10):1260-1271. [doi:10.1109/TPAMI.2004.79]

Zhang, B., Li, Y.F., 2008. A Method for Calibrating the Central Catadioptric Camera via Homographic Matrix. Int. Conf. on Information and Automation, p.972-977. [doi:10.1109/ICINFA.2008.4608140]

Zhang, L., Du, X., Zhu, Y., Liu, J., 2009. Central Catadioptric Camera Calibration with Single Image. IEEE Int. Conf. on Acoustics, Speech and Signal Processing, p.1253-1256. [doi:10.1109/ICASSP.2009.4959818]